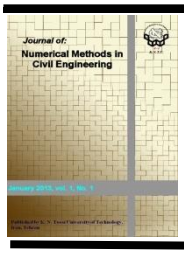

Numerical Methods in Civil Engineering

Optimal placement of post-tensioned self-centering yielding braced systems for braced frame structures

Elnaz Nobahar[*], Behrouz Asgarian[**], Ashkan Torabi Goodarzi[***], Oya Mercan[****]

ARTICLE INFO

Article history:
Received:
July 2019.
Revised:
September 2019.
Accepted:
October 2019.

Keywords:
self-centering systems; post-tensioned wires; residual deformations; energy dissipation; nonlinear dynamic analyses; optimal design

Abstract:

The experience of past prominent earthquakes establishes the fact that the structure's catastrophes and casualties can be dramatically decreased through the use of self-centering systems. A promising post-tensioned self-centering yielding braced system (PT-SCYBS) has been developed, comprising of two main components, including the post-tensioned wires, exhibiting the desirable self-centering properties, and steel bars, providing the energy dissipation capacity. The structural application of such systems is expeditiously expanding due to their capabilities of not only reducing the residual deformations of the structures but also improving the structure's performance level. As such, identifying optimal design and proper placement of the proposed device in the structure is of crucial importance. In this paper, the mechanics of the proposed system, as well as a simple and efficient approach for determining the optimal design of the PT-SCYBS, have been proposed. Numerical models have been employed to examine the effect of various configurations of the device on the hysteretic behavior of the proposed PT-SCYBS. Nonlinear static and dynamic analyses are performed on the seismically deficient 3- and 9-story moment resisting frames (MRFs), enhanced with the optimal placement of the PT-SCYBS. Comparing the results of the PT-SCYBS buildings and MRFs, it can be concluded that the residual drift decreased by 96% and 77% for the 3- and 9-story buildings, respectively. As such, the optimal design of the proposed system in the building causes notably lower residual drifts as compared with the MRF buildings, resulting in enhanced seismic performance.

1. Introduction

The unanticipated and prevailing structural and nonstructural seismic damages of the buildings with conventional lateral force resisting systems highlight the need for pre-disaster techniques to guarantee the inhabitant's safety as well as to prevent damage to the structures during an earthquake. These can be accomplished by means of a number of structural control devices, including the active, semi-active, and passive devices.

**Corresponding Author: Ph.D. Candidate, Faculty of Civil Engineering, K. N. Toosi University of Technology, Tehran, Iran. E-mail: elnaznobahar@email.kntu.ac.ir*
*** Professor, Faculty of Civil Engineering, K. N. Toosi University of Technology, Tehran, Iran.*
**** Ph.D. Student, Department of Mechanical Engineering, Isfahan University of Technology, Isfahan, Iran.*
***** Associate Professor, Department of Civil and Mineral Engineering, University of Toronto, Toronto, Canada.*

In the active and semi-active structural control systems, the response of a building is adjusted by the action of a control system through some external devices such as the power supply, sensors, and hydraulic jack. For active control systems, the sensors provide the required data regarding the behavior of the controlled structure and environmental excitation for the controller. Semi-active systems require only nominal amounts of energy to adjust their mechanical properties, and unlike fully active systems, they cannot add energy to the structure [1]. On the other hand, passive control systems are exceptionally favorable alternatives to semi-active and active systems by providing the advantages of not only reducing the structural energy dissipation demand but also minimizing the damage of the structure. Moreover, unlike semi-active and active systems, the passive control systems, which can be categorized into the rate-dependent and rate-independent devices, do not require high

maintenance costs or any external power supplies. Rate-dependent passive control systems are those whose mechanical responses depend on the rate of the alteration of the displacement across the system. The epitome of such systems is viscoelastic dampers, while the rate-independent ones, such as the hysteresis dampers, are those whose mechanical responses rely on the magnitude of the displacement and the motion direction. Although employing passive energy dissipation systems is a step forward to dissipate the seismic energy through the component's plastic deformation, they are likely to sustain large residual deformations following a severe earthquake. To address this challenge, various earthquake-resilient devices, providing both energy dissipation and re-centering capabilities, have been proposed and verified numerically and experimentally during the last decade [2-7]. The self-centering capability of such devices could bring the structure to its upright position after a seismic event, while their energy dissipation capacity, considered as a primary function, leads to a substantial reduction of the post-seismic demands of the structural components. Consequently, the proper optimal design of such devices may be imperative for improving the post-seismic performance of the structure. Additionally, the extent of the device's contribution to the seismic response of the structure mainly affects the device's functionality by reducing the structural response. As such, the inevitable consequence of the proper distribution and implementation of such devices over the height of structures is the extra damping forces made available for the structures. Various studies have been developed for identifying the optimal locations of the passive control devices in a building structure. Filatrault and Cherry proposed a simplified method for the seismic design of friction dampers as well as an optimization technique to obtain an ideal slip-load distribution of these devices by minimizing a relative performance index (RPI) obtained from energy concepts [8]. Zhang and Soong developed a sequential procedure based on the degree of the controllability concept for finding the optimal locations of viscoelastic dampers in a building, which was then verified by experiments for a five-story building structure. The results showed that the optimization procedure could effectively be applied in controlling the response of the building equipped with viscoelastic dampers [9]. An optimal procedure using a linear quadratic regulator (LQR) was developed by Gluck et al. for the design of the rate-dependent dampers in high-rise buildings. The main goal of their study was to minimize the performance cost function, and create a proper minimal configuration of dampers by maximizing their effects [10]. Takewaki proposed an efficient procedure for establishing the optimal location of viscous dampers in a building with the arbitrary damping system. The main objective of this study was to minimize the sum of the amplitudes of the transfer functions evaluated at the un-damped fundamental natural frequency of a structural system subject to a constraint on the sum of the damping coefficients of added dampers [11]. Wu et al. developed an approach for finding the optimum locations of the three-dimensional structures equipped with passive energy dissipation devices [12]. An optimal procedure was investigated by Shukla et al. for the passive control of viscoelastic dampers when applied to multistory buildings. According to this research, the optimal placement of dampers was found by establishing an index obtained based on the root mean square (RMS) value of the story drifts [13]. Garcia proposed a new algorithm, called a simplified sequential search algorithm for finding an optimal configuration of dampers, in which dampers were placed sequentially to achieve the maximum efficiency. Afterward, a numerical simulation was developed, the results of which revealed, that the proposed approach was significantly effective in controlling the response of the building [14]. Moreschi et al. developed a methodology using the genetic algorithm for obtaining the optimal design parameters of yielding metallic and friction dampers [15]. Meanwhile, Asahina et al. developed a genetic algorithm-based approach for obtaining the optimum distribution of linear viscous dampers in two- and three-dimensional building structures. The results clarified significant reductions in the story drift and absolute accelerations relative to the uniform placement of dampers [16]. Lavan et al. developed a new approach for the optimal design of added viscous damping for a suite of ground motion records with a constraint on the maximum drift [17]. More recently, to identify the optimum positions of fluid viscous dampers in a three-dimensional structure with an arbitrary degree of complexity in the configuration, an approach was investigated by Kokil et al. [18]. The optimum function was a linear combination of the maximum story drift and maximum base shear of the damped structure normalized by their respective un-damped counterparts. Sanghai et al. formulated a general framework for the optimal location of friction dampers in unsymmetrical reinforced concrete buildings [19]. The results illustrated that the proposed methodology has notable effects on the response reduction of the buildings. In this paper, an optimization-based approach is proposed for the optimal design of a novel post-tensioned self-centering yielding braced system (PT-SCYBS). This ideal scheme is efficient and straightforward enough so that, the proposed configuration of the device minimizes the extent of excessive devices that a structure requires, to reach a given performance level. In this study, the mechanics and behavior of the PT-SCYBS are first described. Then, a simple optimization approach is proposed to find the optimal design of the device. An analytical study is employed to assess the hysteretic behavior of the optimized PT-SCYBS as well as to evaluate the effect of different configurations of the

device, i.e., the placement and number of devices on the seismic response of the structure. Finally, a numerical study is conducted to investigate the efficiency of the proposed device in 3- and 9-story braced frame buildings.

2. Hysteretic behavior of the PT-SCYBS

A PT-SCYBS is a new form of self-centering energy dissipation systems that can be categorized as a passive control system in new or existing buildings, mounting to the structures similar to other conventional braces, as shown in Figure 1.

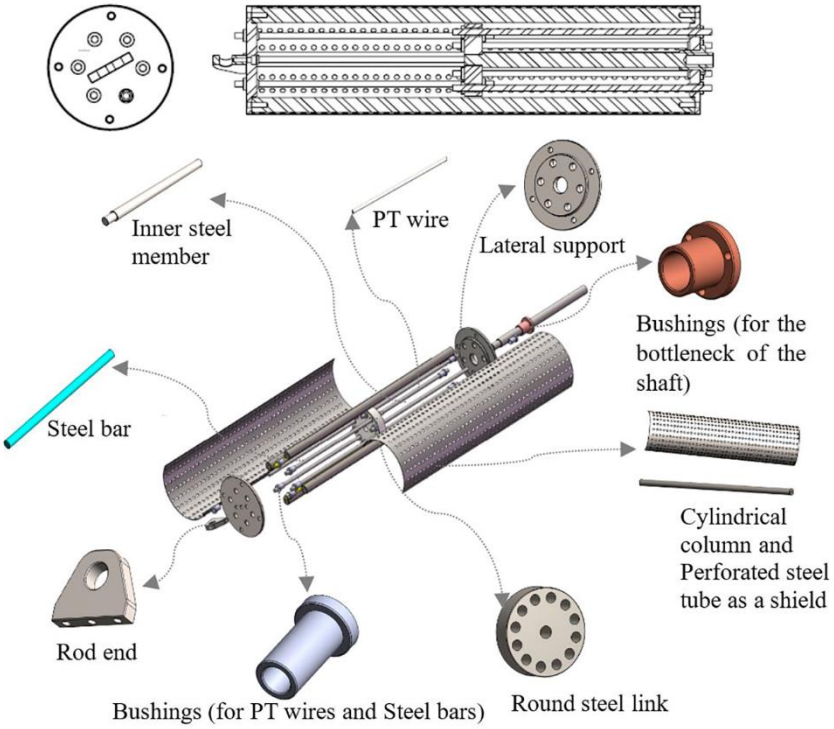

Fig. 1: The proposed PT-SCYBS and its components [20]

This damage-resistance system takes advantage of two mechanisms assembled in parallel, including a restoring force mechanism that can return the building to its upright position along with an enhanced energy dissipation behavior to produce a flag-shaped hysteresis response as shown in Figure 2. Further details regarding the mechanics of the PT-SCYBS can be found in the work of Nobahar et al. [20], which are not discussed here on the grounds of conciseness. It is to be noted that the post-tensioned (PT) wires have been applied in the device for their re-centering property, while the use of steel bars as an energy dissipative (ED) component seems inevitable due to the negligible energy dissipation capacity of the post-tensioned wires. Consequently, the complete hysteretic behavior of the PT-SCYBS can be achieved by adding the hysteresis responses of the PT wires and steel bars, as shown in Figure 2(c), in which k_i is the initial stiffness of the PT-SCYBS; P_{act} and δ_{act} account for the activation force and the corresponding activation displacement of the PT-SCYBS.

3. Optimal proportion of the PT-SCYBS

One of the main reasons for employing PT-SCYBSs in the structure is its high self-centering and energy dissipating capabilities. During the seismic loading, the self-centering capability of the device brings the structure to its original condition, which consequently prevents the accumulation of plastic deformation in the structure.

Nevertheless, the energy dissipation capacity decreases the structural demands by reducing the probability of the formation of plastic hinges in the structure. With regard to the mentioned presumptions, the primary goal of designing the optimized device would be maximizing the energy dissipation capacity while maintaining the self-centering capability. Thus, specifying an optimized amount of both PT wires and steel bars results in an excellent performance of the device. In this regard, a simple, efficient, and practical objective function, assumed as a linear combination of two specific ratios, was developed for identifying an optimal design of the PT-SCYBS as follows:

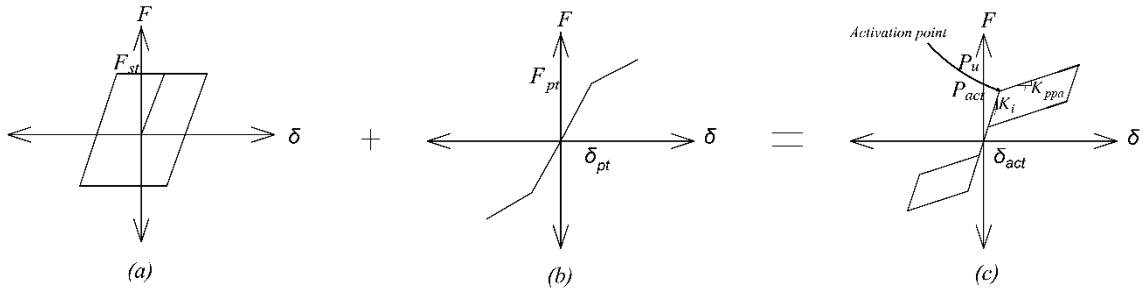

Fig. 2: Hysteresis behaviour of the (a) steel bar, (b) PT wire, (c) PT-SCYBS [20]

$$function = \frac{E_{damped\cdot PT-SCED}}{E_{damped\cdot ED}} - \frac{\varepsilon_{res\cdot PT-SCED}}{\varepsilon_{res\cdot ED}} \quad (1)$$

where $\frac{E_{damped\cdot PT-SCED}}{E_{damped\cdot ED}}$ is the energy dissipation ratio, defined as the maximum amount of energy dissipated by the PT-SCYBS, normalized by the amount of energy dissipated by the ED part, i.e., steel bars; $\frac{\varepsilon_{res\cdot PT-SCED}}{\varepsilon_{res\cdot ED}}$ accounts for the self-centering ratio, specified as the maximum amount of the residual deformation of the PT-SCYBS, normalized by the amount of residual drift of the ED part. As such, the proposed function has been considered to incorporate both the energy dissipation and self-centering capabilities of the PT-SCYBS. As shown in Figure 3, the objective function was developed for a specific number of steel bars and PT wires.

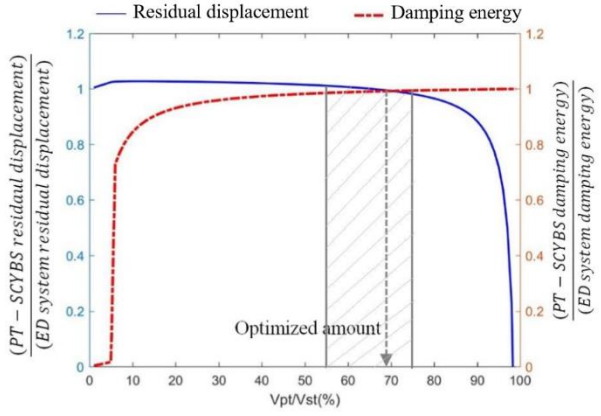

Fig. 3: Sample of the objective function for determining the optimum ratio of the 9-story building with the PT-SCYBS [20]

Besides, with reference to the objective function, the optimized number and diameters of steel bars and PT wires for the design of the PT-SCYBS are summarized in Table 1. It is worth noting that the number and diameter of the optimized PT wires and steel bars were calculated such that not only the dissipated energy of the PT-SCYBS was maximized, but also the residual drifts of the proposed system were minimized. Moreover, to precisely evaluate the objective function, the upper and lower bounds of the optimum amount were also established. As can be seen in the results of the first group, the amount of energy damped by the PT-SCYBS was more substantial than that of the ED system, whereas the residual drift of the PT-SCYBS was extremely lower compared to the ED system. Furthermore, a comparison was made between the results of the optimum amount and the lower bound. As highlighted, although no significant changes were observed between the normalized ratios of the energy dissipation, the PT-SCYBS resulted in achieving residual drifts of nearly 50% of those reached by the ED systems. Moreover, the lower the ratio of the residual drift of the PT-SCYBS to that of the ED system, the higher the volume ratio of the PT wires to steel bars. However, from the economical perspective, employing large number of PT wires results in high costs, which may not be practical and affordable. Additionally, changing the number and diameter of the steel bars and PT wires may affect the amount of energy dissipation and residual drifts of the optimized PT-SCYBS. As can be seen, increasing the number of steel bars and leaving the other parameters fixed; i.e., the number of steel bars and PT wires, and the diameter of post-tensioned wires, resulted in an unremarkably improved (about 0.19% in average) damped energy ratio of the PT-SCYBS to the ED system. On the other hand, the residual drift ratio of the PT-SCYBS to the ED system significantly increased with an average of 45%. Moreover, increasing the diameter of steel bars and leaving other parameters fixed resulted in a negligible increase in the energy dissipated ratio of the PT-SCYBS to the ED system (about 0.18% on average). However, increasing the steel bar diameter may have a significant effect on the residual drift reduction of the PT-SCYBS compared with that of the ED system (about 47% on average).

Table 1. The optimized amount of Energy dissipation and Self-centering parts of the PT-SCYBS

Group	Item	Steel bars		PT wires		Optimum amount	Energy Part			Self-centering Part		
		Number	Diameter (mm)	Number	Diameter (mm)	%Vpt/Vst	PT-SCYBS Damping Energy	ED Damping Energy	Ratio	PT-SCYBS Residual Disp.(mm)	ED Residual Disp. (mm)	Ratio
1	a	4	8	4	10	61	1.29E+04	1.26E+04	1.031	4.95E-02	7.1	0.007
	b	4	8	8	6	53	1.30E+04	1.26E+04	1.034	6.84E-02	7.1	0.01
2	a	4	10	8	6	43	2.03E+04	1.96E+04	1.036	1.03E-01	7.1	0.015
	b	4	10	4	10	50	2.03E+04	1.96E+04	1.035	7.74E-02	7.1	0.011
3	a	4	12	12	6	43	2.93E+04	2.82E+04	1.036	1.03E-01	7.1	0.015
	b	4	12	6	10	51	2.92E+04	2.82E+04	1.035	7.42E-02	7.1	0.011
4	a	6	12	12	6	34	4.40E+04	4.24E+04	1.038	1.50E-01	7.1	0.021
	b	6	12	10	10	54	4.38E+04	4.24E+04	1.034	6.58E-02	7.1	0.009
5	a	6	10	10	6	37.6	3.05E+04	2.94E+04	1.037	1.28E-01	7.1	0.018
	b	6	10	6	10	50	3.04E+04	2.94E+04	1.035	7.74E-02	7.1	0.011
6	a	6	8	8	6	43	1.95E+04	1.88E+04	1.036	1.03E-01	7.1	0.015
	b	6	8	8	10	67.6	1.94E+04	1.88E+04	1.028	3.71E-02	7.1	0.005

4. Hysteresis response of the PT-SCYBS

4.1. Hysteretic behavior of the post-tensioned wires

To develop the hysteretic behavior of the PT wires, cyclic tests of the PT wires have been conducted using a universal testing machine. In the current study, a loading history was adopted for the cyclic analyses based on FEMA 461 [21] (Figure 4(a)). As can be seen from the results, a satisfactory agreement has been observed between the numerical and experimental results (Figure 4(b)).

4.2. Hysteretic response of the PT-SCYBS

To simulate the hysteretic behavior of the PT-SCYBS, the Open Systems for Earthquake Engineering Simulation (OpenSees) Framework [22] has been employed. As shown in Figure 5, the FEMA 461 loading protocol that has been applied, contains increasing step-wise cycles of deformation amplitudes, in which two cycles at each amplitude must be completed.

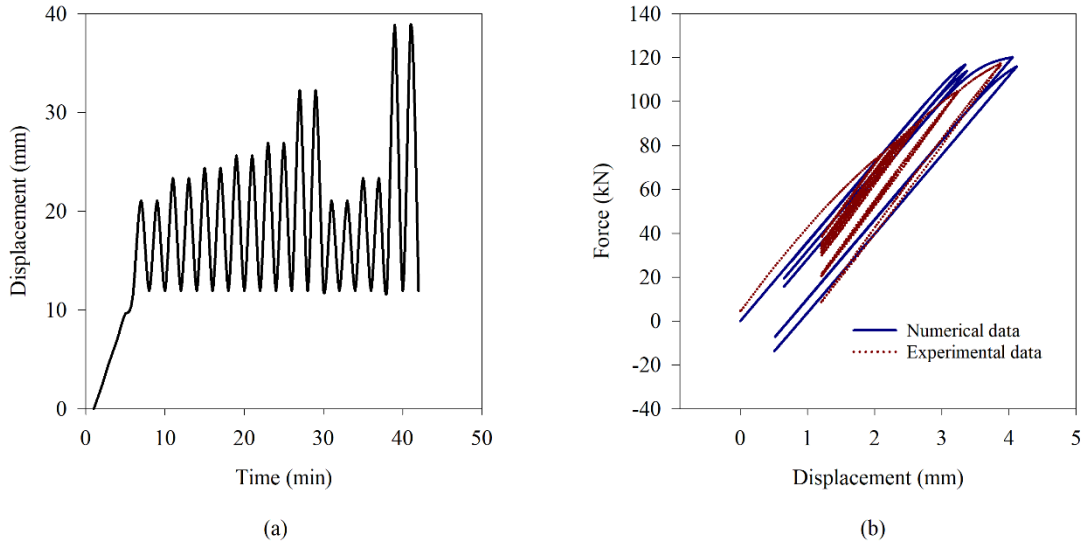

Fig. 4: (a) The cyclic loading protocol of the PT wires, (b) Experimental and numerical verification of the cyclic responses

To model the PT wires, an "ElasticMultiLinear" material of OpenSees has been considered along with the "InitStressMaterial" material model for the pretensioning force of the PT wires. To model the steel bars of the proposed system, the "Steel02" material model has been assigned with a modulus of elasticity and an isotropic hardening ratio of 200000 MPa and 0.005, respectively. Besides, two "ElasticPPGap" material models functioning in parallel have been considered to simulate the contact between the steel bars and the central plate. Further information on the computational model of the proposed system can be found in the work of Nobahar et al. [20], which is not presented here for the sake of brevity.

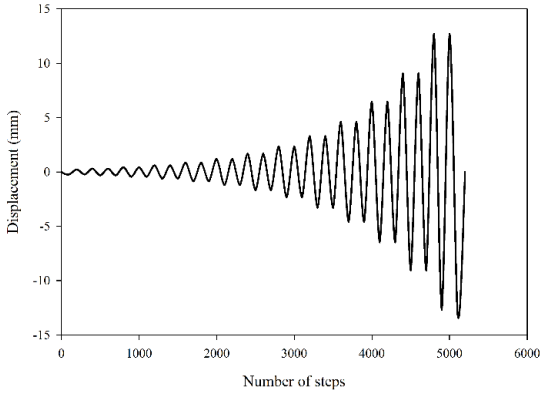

Fig. 5: The Cyclic loading protocol for the PT-SCYBS, based on FEMA 461[21]

4.3. Results and discussion

The force-deformation hysteretic responses of the proposed system under cyclic loading for various optimal volume ratios of PT wires to steel bars are demonstrated in Figures 6 to 11.

As noted, a symmetrical behavior of the PT-SCYBS under tensile and compressive forces was observed, revealing a unique and appealing property of the PT-SCYBS. Besides, the PT-SCYBS exhibited quite stable and repeatable loops with no strength and strain degradation, specifying the high efficiency of the PT-SCYBS in decreasing the residual drifts of the structure. Figure 12 shows a parallelogram hysteresis curve of the yielding component, possessing a symmetrical behavior under both tensile and compressive forces.

The effect of the diameter and the number of steel bars on the PT-SCYBS cyclic behavior is shown in Figure 13. It is to be noted that samples 1 and 2 refer to the PT-SCYBS with an identical SC component, i.e., 12 PT wires of 6mm diameter, and different ED components, i.e., four and six steel bars of 12mm diameter respectively. Furthermore, samples 3 and 4 account for the PT-SCYBS with an identical self-centering component, i.e., four PT wires of 10mm diameter, and different ED components, i.e., four steel bars of 8mm and 10mm diameters respectively. Accordingly, as the number and diameter of steel bars increases, the damping energy of the PT-SCYBS, i.e., the area under the hysteresis curve, improves.

5. PT-SCYBS placement optimization

5.1. Selection of ground motions

In this study, three suites of earthquake ground motions of Los Angeles, Boston, and Seattle have been considered. Every individual suit developed by Somerville et al. in the SAC steel project [23] includes 20 records and corresponds to a 2% probability of exceedance in a 50-year period.

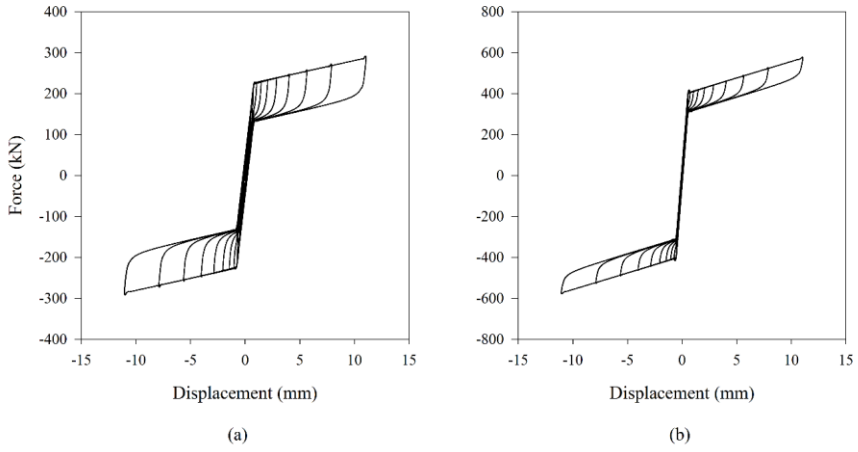

Fig. 6: The hysteretic response of the PT-SCYBS under cyclic loading with 4 steel bars of 8mm diameter and (a) 4 post-tensioned wires of 10 mm diameter, (b) 8 post-tensioned wires of 6 mm diameter

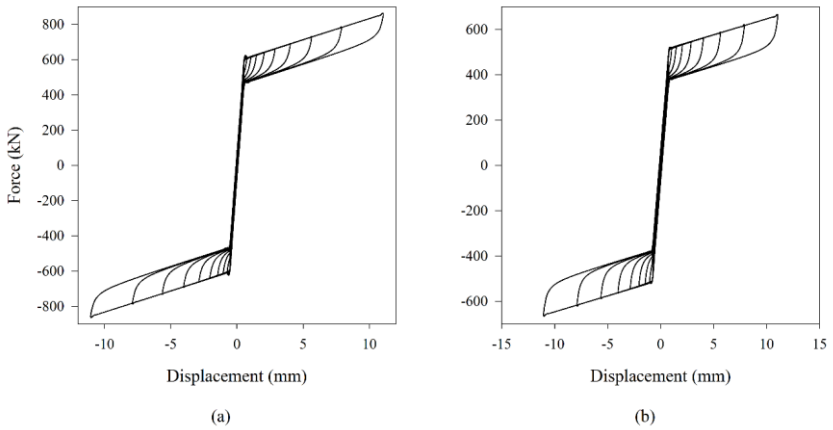

Fig. 7: The hysteretic response of the PT-SCYBS under cyclic loading with 4 steel bars of 10mm diameter and (a) 8 post-tensioned wires of 6 mm diameter, (b) 4 post-tensioned wires of 10 mm diameter

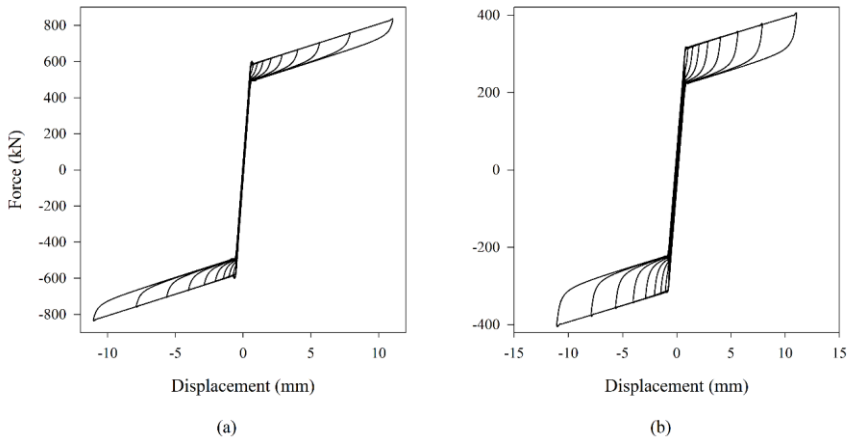

Fig. 8: The hysteretic response of the PT-SCYBS under cyclic loading with 4 steel bars of 12mm diameter and (a) 12 post-tensioned wires of 6 mm diameter, (b) 6 post-tensioned wires of 10 mm diameter

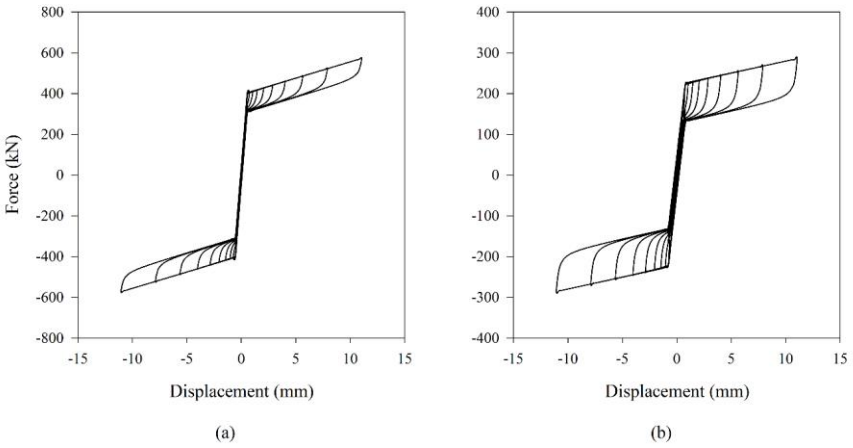

Fig. 9: The hysteretic response of the PT-SCYBS under cyclic loading with 6 steel bars of 12mm diameter and (a) 12 post-tensioned wires of 6 mm diameter, (b) 10 post-tensioned wires of 10 mm diameter

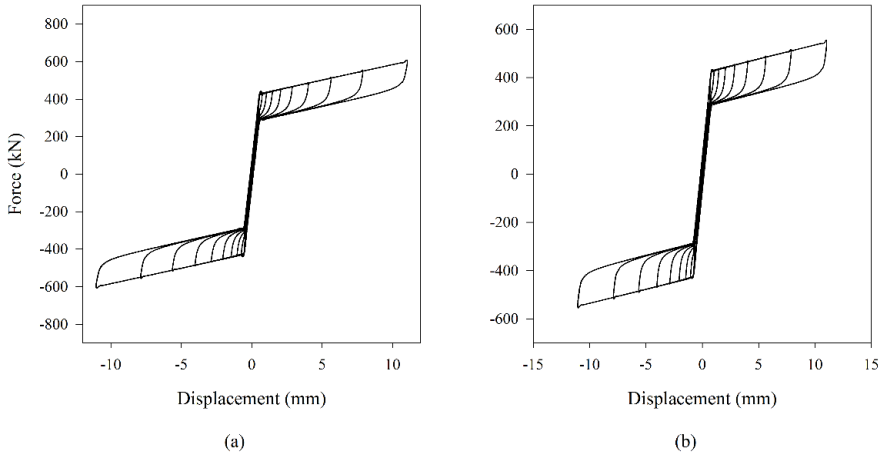

Fig. 10: The hysteretic response of the PT-SCYBS under cyclic loading with 6 steel bars of 10mm diameter and (a) 10 post-tensioned wires of 6 mm diameter, (b) 6 post-tensioned wires of 10 mm diameter

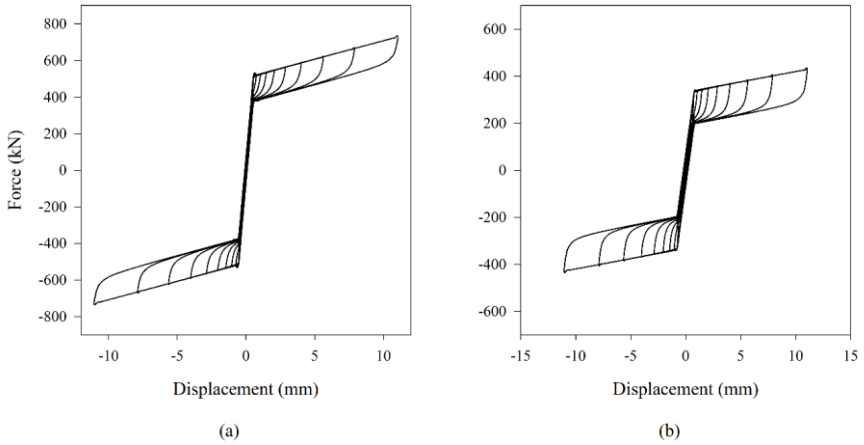

Fig. 11: The hysteretic response of the PT-SCYBS under cyclic loading with 6 steel bars of 8mm diameter and (a) 8 post-tensioned wires of 6 mm diameter, (b) 8 post-tensioned wires of 10 mm diameter

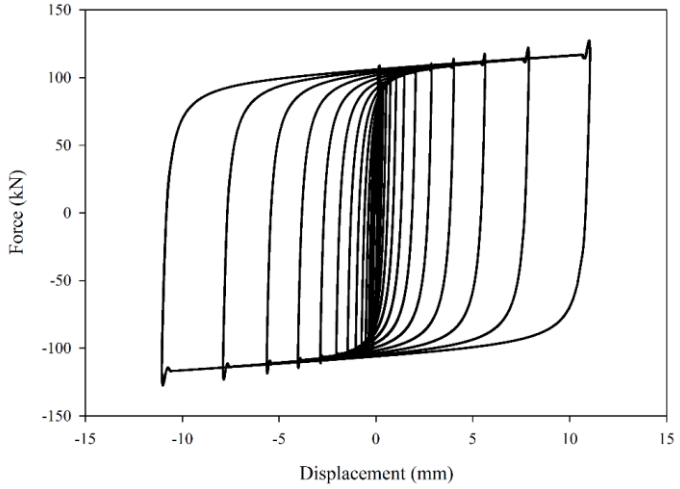

Fig. 12: Hysteretic behavior of steel bars of 10mm diameter

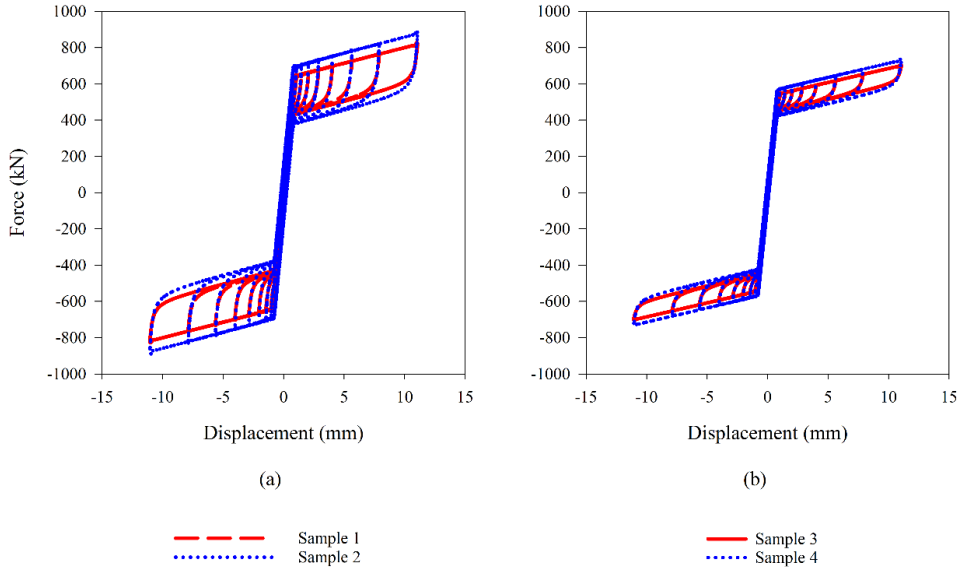

Fig. 13: The effect of (a) the diameter of the steel bars for samples 1 and 2, (b) the number of steel bars for samples 3 and 4 on the PT-SCYBS hysteretic behavior

5.2. Building description

To evaluate the seismic performance of the PT-SCYBS, the 3-story and 9-story PT-SCYBS braced frame buildings were considered and compared with moment resisting frames, primarily designed for the SAC Phase II steel project. The 3- and 9-story buildings illustrated the low- and mid-rise benchmark buildings located in Los Angeles, California. It is to be noted that the 3- and 9-story steel structures with the proposed PT-SCYBS were designed such that the overall characteristics considered were identical to those of the moment-resisting frames. The lateral load resisting system of both buildings consists of steel moment-resisting frames, while their interior system comprises of simple frames with composite floors. The story height of the 3-story building was 13 ft (3.96 m). However, concerning the 9-story building, the story height of the structure was 13ft (3.96m), excluding the basement and ground-level stories, which were 12 ft (3.65m) and 18ft (5.49m), respectively. Furthermore, the plan dimension of the 180x120 ft^2 3-story buildings contained a 30ft (9.15m) (four-bay in the X-direction) by 9.15m (five-bay in the Y-direction). While the plan dimension of the 150x150 ft^2 9-story buildings contained 30ft (9.15m) (four-bay in the X- and Y-direction). The sections of beams and columns of 3- and 9-story buildings were demonstrated in Tables 2 and 3. The wide flange sections of beams and columns comprised of grade 36 and 50 steel, respectively. It is to be noted that the seismic mass of the 3- and 9-story structures were 2.95e4 and 9.0e4 kN, respectively.

5.3. Different configurations of the PT-SCYBS

To optimize the effect of the PT-SCYBS on the structural response of the 3- and 9-story buildings, several configurations and arrangements of the device were examined. It is to be noted that the proposed device can be installed as a diagonal configuration, as well as strongback braced configuration, proposed by Mahin et al. [24]. With regard to 3-story buildings, the angle between the PT-SCYBS and the horizontal axis was 23.43 degrees, while the mentioned angle was 23.43 and 30.96 degrees for the location of the damper in the first story and other stories of the 9-story building, respectively. As shown in Figures 14 and 15, several distributions of three and six PT-SCYBSs in the 3-story building, as well as four and eight PT-SCYBSs in the 9-story building, were considered. In this study, the PT-SCYBSs have been diagonally induced in the structures with few fixed location patterns, choosing arbitrarily so as to reach the least number of the proposed system. It is to note that using different configurations with different numbers of the PT-SCYBSs in the building frame is feasible, keeping their total quantity the same.

Table 2. Design characteristics of 3-story braced frame building archetypes

3-story braced frame building						
Story	NS Moment resisting frame			NS gravity frame		
	Columns		Girders	Columns		Beams
	Exterior	Interior		Below penthouse	Other columns	
1	w14x176	w14x211	w30x90	w14x82	w14x68	w18x35
2	w14x176	w14x211	w27x84	w14x82	w14x68	w18x35
3	w14x176	w14x211	w21x50	w14x82	w14x68	w16x26

Table 3. Design characteristics of 9-story braced frame building archetypes

9-story braced frame building						
Story/Level	NS Moment resisting frame			NS gravity frame		
	Columns		Girders	Columns		Beams
	Exterior	Interior		Below penthouse	Other columns	
Ground level	w14x257	w14x342	w33x118	w14x211	w14x193	w21x44
1	w14x257	w14x342	w33x118	w14x211	w14x193	w18x35
2	w14x257	w14x342	w33x118	w14x211	w14x193	w18x35
3	w14x257	w14x311	w30x99	w14x159	w14x145	w18x35
4	w14x257	w14x311	w30x99	w14x159	w14x145	w18x35
5	w14x193	w14x257	w30x99	w14x120	w14x109	w18x35
6	w14x193	w14x257	w30x99	w14x120	w14x109	w18x35
7	w14x176	w14x193	w24x76	w14x90	w14x82	w18x35
8	w14x176	w14x193	w24x62	w14x90	w14x82	w18x35
9	w14x159	w14x176	w21x50	w14x61	w14x82	w16x26

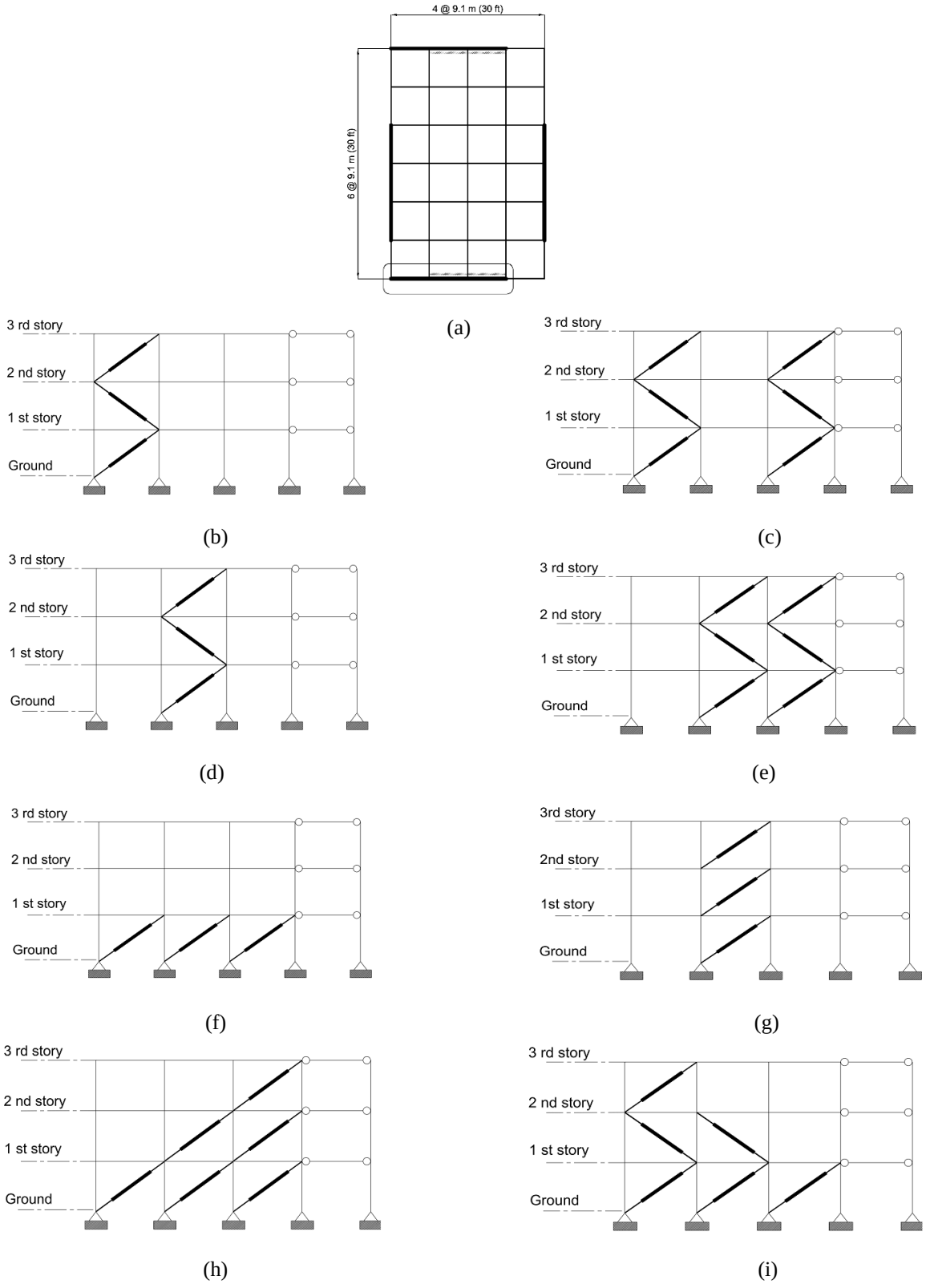

Fig. 14: Various distributions of the 3-story building with 3 and 6 dampers. (a) plan (b) conf.3-3-1 (c) conf.3-6-1 (d) conf.3-3-2 (e) conf.3-6-2 (f) conf.3-3-4 (g) conf.3-3-3 (h) conf.3-6-3 (i) conf.3-6-4

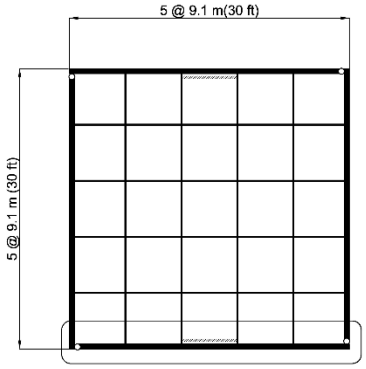
5 @ 9.1 m(30 ft)
5 @ 9.1 m (30 ft)

(a)

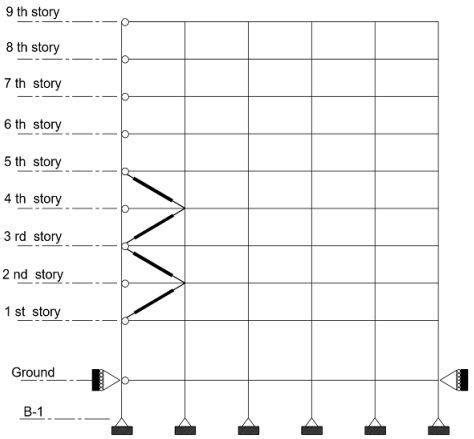
9 th story
8 th story
7 th story
6 th story
5 th story
4 th story
3 rd story
2 nd story
1 st story
Ground
B-1

(b)

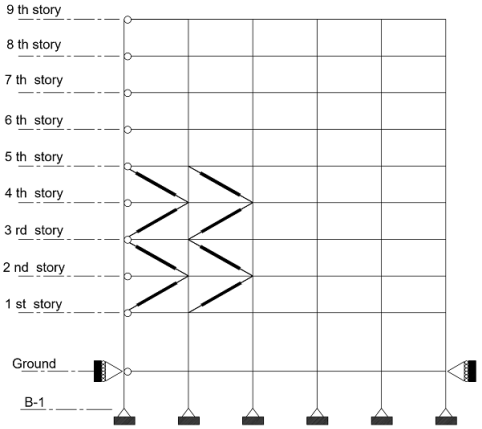
9 th story
8 th story
7 th story
6 th story
5 th story
4 th story
3 rd story
2 nd story
1 st story
Ground
B-1

(c)

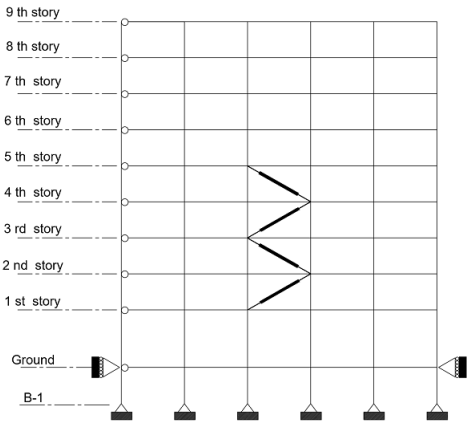
9 th story
8 th story
7 th story
6 th story
5 th story
4 th story
3 rd story
2 nd story
1 st story
Ground
B-1

(d)

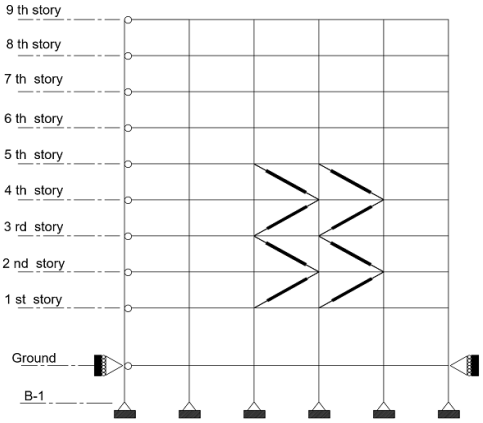
9 th story
8 th story
7 th story
6 th story
5 th story
4 th story
3 rd story
2 nd story
1 st story
Ground
B-1

(e)

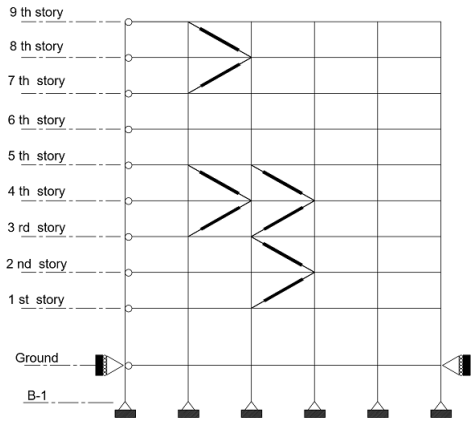

(f)

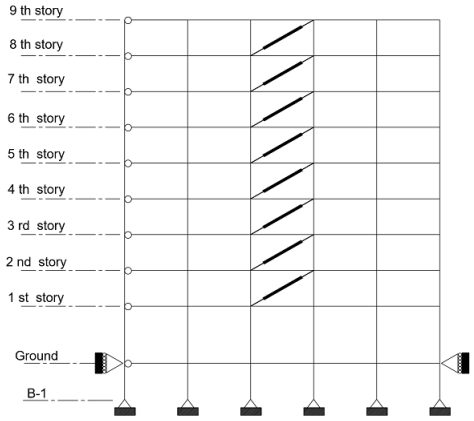

(g)

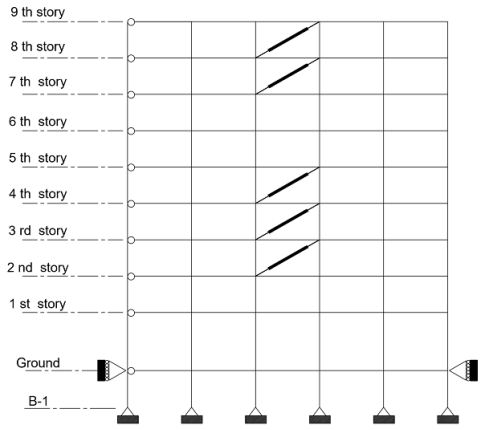

(h)

Fig. 15: Various distributions of the 9-story building with 4 and 8 dampers. (a) plan (b) conf.9-4-1 (c) conf.9-8-1 (d) conf.9-4-2 (e) conf.9-8-2 (f) conf.9-8-3 (g) conf.9-4-3 (h) conf.9-8-4

To assess the structural response of all configurations, nonlinear time history analyses were conducted under three sets of ground motions. The optimal configuration of the PT-SCYBS was determined by applying a drift index, α_i, specifying the effect of different configurations on the drift reduction. The value of α_i identifies the efficiency of the proposed PT-SCYBS during the seismic loading. As such, the lower the α_i index, the higher the re-centering capability of the PT-SCYBS.

$$\alpha_i = \frac{\Delta_{ij}}{\Delta_{io}} \quad (2)$$

where Δ_{ij} accounts for the maximum residual drift of the j^{th} configuration at the i^{th} story, and Δ_{i0} denotes the maximum residual drift of a structure without any PT-SCYBSs at the i^{th} story. Figure 16 presents the results of different configurations of the 3-story buildings under three sets of ground motions with a probability of 2% in 50-year, i.e., maximum considered earthquake. As shown in Figure 16, the results of the 3-story structure with three and six PT-SCYBS devices highlighted that the maximum response reduction was obtained for the strongback braced configurations, i.e., configurations 3-3-2 and 3-6-2, respectively. Furthermore, the average drift reduction of the 3-story buildings with three and six PT-SCYBS devices was 70% and 85% compared to the moment-resisting frame building, respectively, revealing the efficacy of the location of the PT-SCYBSs in reducing the seismic response of the structure.

Additionally, the results for the 9-story structure with four and eight PT-SCYBS devices are demonstrated in Figure 17.

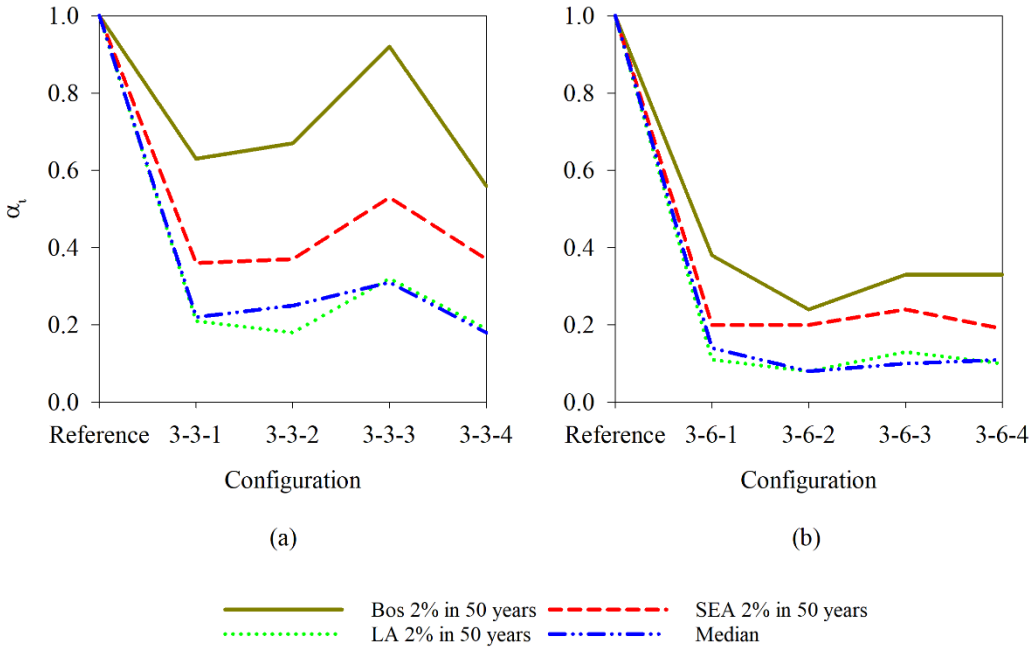

Fig. 16: The effect of damper's configurations for the 3-story building under three sets of ground motions. (a) three sets of devices, (b) six sets of devices

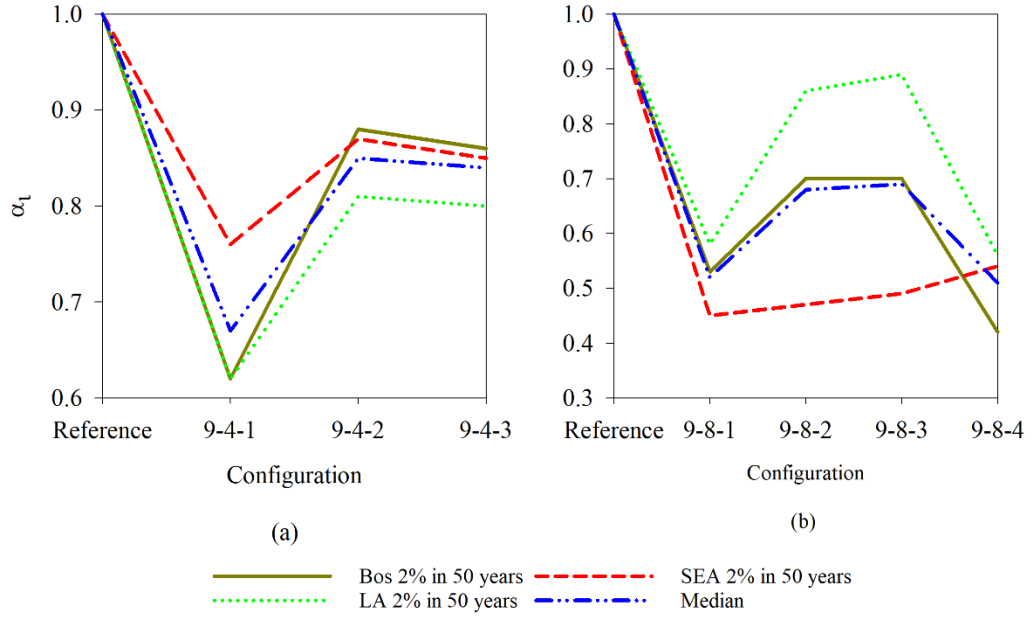

Fig. 17: The effect of damper's configurations for the 9-story building under three sets of ground motions (a) four sets of devices. (b) eight sets of devices

As noted in the results, for the 9-story structure equipped with four PT-SCYBSs, the strongback-braced configuration, i.e., configuration 9-4-1, provided the most significant response reduction, while the diagonal configuration, i.e., configuration 9-8-4, had an improved efficiency in decreasing the seismic response of the 9-story building in term of residual drifts. Besides, the reduction of residual drifts for buildings with four and eight PT-SCYBS devices was 33% and 49%, respectively, when compared with the 9-story moment resisting frame building. Moreover, to further evaluate the effectiveness of the proposed optimization approach, the most effective configuration of the 3- and 9-story structures equipped with the optimum PT-SCYBS, possessing the maximum response reduction, were summarized in Figure 18. As can be seen, the structure with optimally placed PT-SCYBSs provided lower α_i, and thus lower residual drifts as compared to the structure with non-optimal configuration.

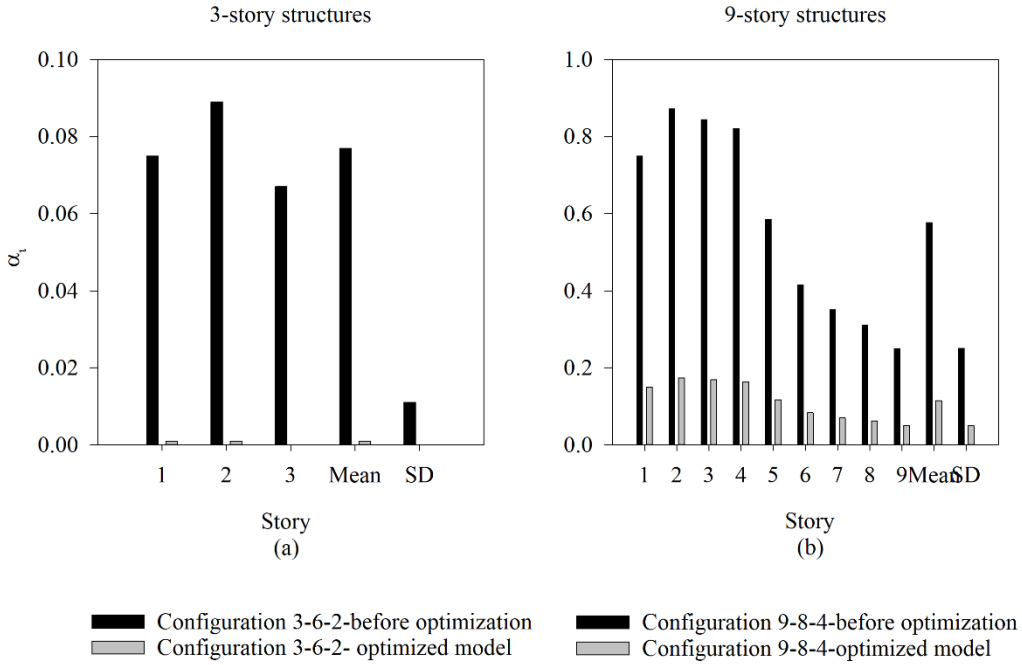

Fig. 18: The value of α_i before and after optimization at 2% in a 50-year earthquake for (a) the 3-story buildings, and (b) the 9-story buildings

6. Nonlinear static pushover analysis

To assess the global behavior of the buildings, nonlinear static analyses were performed according to the lateral load distribution of FEMA 356 [25]. With regard to the p-delta effect, the gravity load was applied to the structures prior to applying the lateral loads. To remark the p-delta effect, the target displacement was considered to be equal to 6% of the roof drift, which could probably be adequate to extract the structure into the inelastic range. Figure 19 shows the results for the PT-SCYBS buildings, i.e., configurations 3-6-2 and 9-8-4, in terms of the base shear and the roof drift ratio along with their yielding point, in which the "equal energy" concept of the bi-linear method was applied.

As noted, a bilinear behavior through the specified displacement range was observed in both base shear and roof drift ratio. Moreover, the design-level drift limit was marked on each building's curve, according to ASCE7-16 [26]. Table 4 summarizes the pushover parameters, including the full yielding base shear, defined at the onset of the global mechanism of the structure, and the design base shear specified the base shear at the ASCE7-16 drift limit.

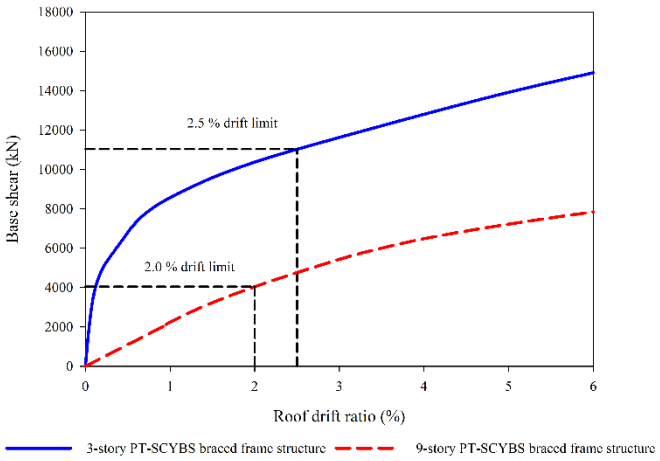

Fig. 19: The pushover curves of the 3- and 9-story braced frame buildings equipped with PT-SCYBSs

Table 4. The pushover parameters for 3- and 9-story buildings

Structural building characteristics				
Number of story	T_1	V_y	⍰$_y$	V_d
MRF building				
3	1.07	676.31	1.28	686.5
9	2.04	1488.77	0.84	1513.01
Braced frame building				
3	0.73	1977.45	0.41	2479.23
9	1.58	1206.27	2.12	908.54

As can be seen from the results, the fixed base columns of the 3-story structures, inducing an improved base shear response, resulted in an enhanced strength of 3-story PT-SCYBS structures compared to the corresponding 9-story PT-SCYBS structures. Additionally, the stiffness reduction of both 3- and 9-story PT-SCYBS structures emerged through the yielding of the PT wires. Besides, due to the presence of PT wires in the 3- and 9-story PT-SCYBS structures, their overall behavior was maintained without any strength degradation after the yielding point. It is worth mentioning that the p-delta effect was directly proportional to the height of the building, and consequently, the higher the height of the structure, the lower the structural post-yield stiffness.

7. Nonlinear dynamic analysis

To assess the efficiency of the proposed PT-SCYBS, the nonlinear dynamic analyses were conducted for the 3- and 9-story moment resisting frame and PT-SCYBS braced frame buildings under a suite of seismic ground motions. As illustrated in Figures 20 and 21, the maximum drift ratio and residual drift ratio were examined for the mentioned buildings.

As highlighted, the 3- and 9-story PT-SCYBS buildings, i.e., configuration 3-6-2 and 9-8-4, respectively, included lower maximum story drifts as compared to the corresponding moment-resisting frame buildings. As such, for the 3- and 9-story PT-SCYBS buildings, the reduction of story drifts was 86 and 68% on average, respectively, conceding the remarkably improved performance of the PT-SCYBS buildings. In addition, concerning the residual drift ratio, employing the PT-SCYBSs results in decreasing the residual drift ratio by 96% and 77% for 3- and 9-story buildings, respectively. Besides, Figure 22 shows the 50th percentile roof displacement of the 3-story PT-SCYBS and moment-resisting buildings under the maximum considered earthquake suite (i.e., with 2% probability in a 50-year).

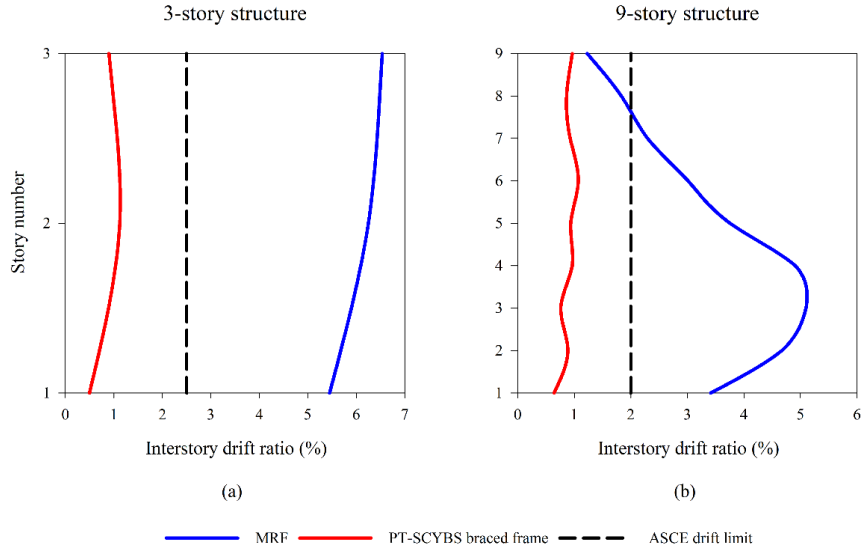

Fig. 20: Peak story drift ratios at 2% in a 50-year earthquake for buildings equipped with PT-SCYBSs (a) 3-story buildings, (b) 9-story buildings

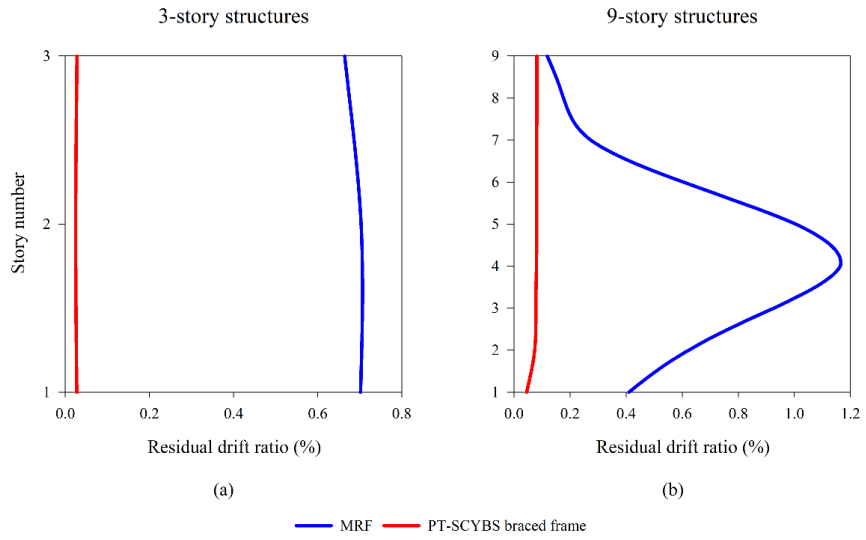

Fig. 21: Residual drift ratios at 2% in a 50-year earthquake for buildings equipped with PT-SCYBSs (a) 3-story buildings, (b) 9-story buildings

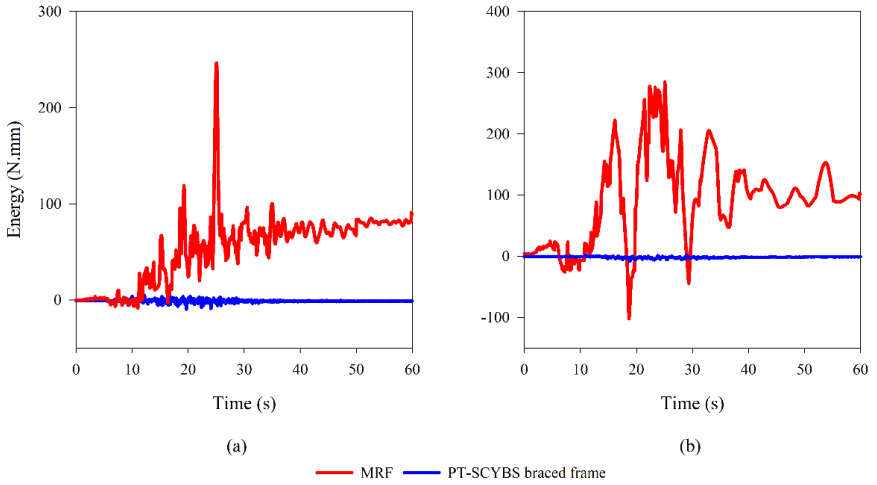

Fig. 22: The median roof displacement at 2% in a 50-year earthquake for buildings equipped with PT-SCYBSs (a) 3-story buildings, (b) 9-story buildings

As can be seen, the maximum roof displacement of the 3- and 9-story PT-SCYBS buildings considerably reduced as compared to their reference moment-resisting frame buildings, in which decreasing the maximum roof displacement were 98 and 92 % on average respectively. Figures 23 and 24 show the contribution of various extents of the energy of the 3- and 9-story structures.

According to the results, the PT-SCYBS played a significant effect on dissipating the total input energy of the 3- and 9-story PT-SCYBS structures. As such, the damped energy ratios of the 3- and 9-story PT-SCYBS structures to the corresponding moment-resisting frame structures were 2.34 and 2.2, implying the vital importance of the PT-SCYBS in enhancing the performance level of the structure.

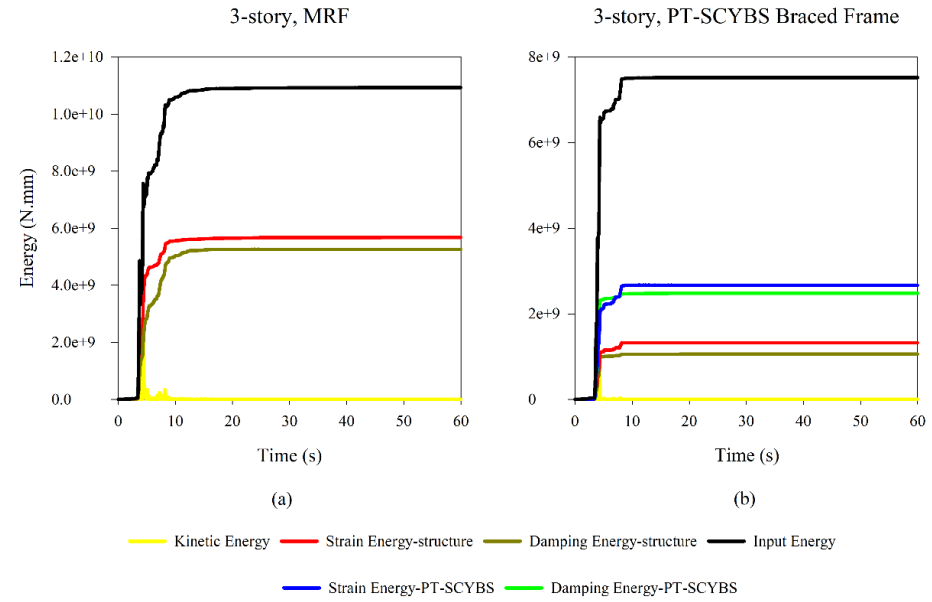

Fig. 23: The contribution of different energy parts in the (a) 3-story MRF building, (b) 3-story braced frame building

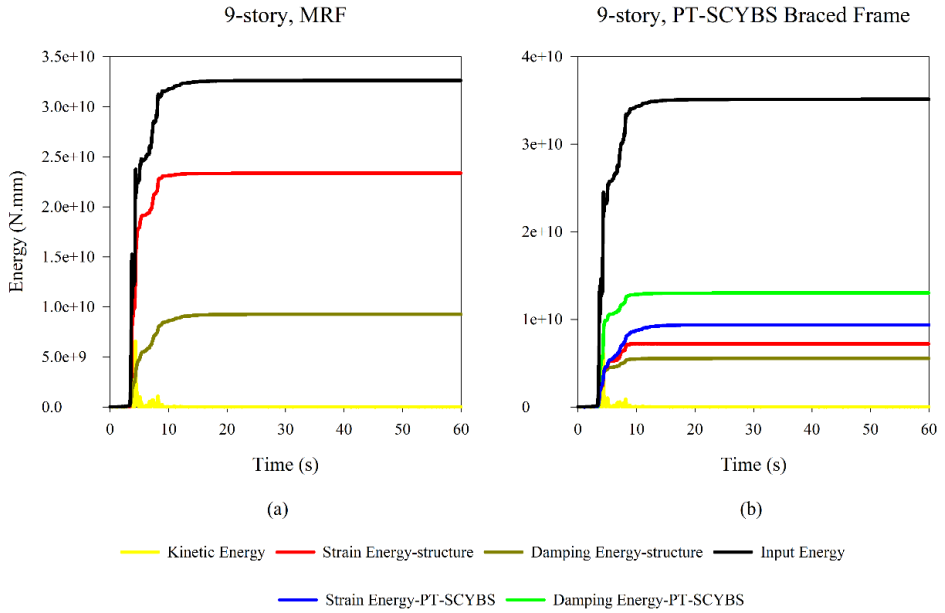

Fig. 24: The contribution of different energy parts in the (a) 9-story MRF building, (b) 9-story braced frame building

8. Conclusions

This research presents a novel bracing system called post-tensioned self-centering yielding braced system (PT-SCYBS), which can be typically installed as a part of bracing systems to resist the lateral seismic load. First, the mechanics of the proposed system were presented. Then, the hysteretic response of the PT-SCYBS was examined under the cyclic loading protocol developed by FEMA 461. The results certify that the proposed system demonstrated a flag-shaped hysteretic response with repeatable hysteresis loops. Moreover, an analytical study was conducted to obtain the optimum placement of the proposed system in the building by examining different configurations. Finally, a comparative study of the PT-SCYBS buildings and the MRFs was conducted, which was based on the nonlinear static and dynamic analyses of the 3- and 9-story buildings. The nonlinear dynamic analysis was conducted on three suites of earthquake ground motions representing the maximum considered earthquake (MCE). The pushover analysis results revealed the improved nonlinear lateral load behavior of the PT-SCYBS structures. Comparing the results of the structures equipped with the PT-SCYBS and the MRF structures, it

can be revealed that the ratio between the residual drifts of the 3- and 9-story PT-SCYBS and MRF buildings is equal to 0.02 and 0.09, respectively, highlighting the exceptional seismic performance of the buildings equipped with the optimally designed PT-SCYBSs.

References

[1] T.T. Soong, G.F. Dargush, Passive energy dissipation systems in structural engineering, Wiley1997.

[2] C. Christopoulos, R. Tremblay, H.-J. Kim, M. Lacerte, Self-centering energy dissipative bracing system for the seismic resistance of structures: development and validation, Journal of structural engineering, 134 (2008) 96-107.

[3] M.R. Eatherton, L.A. Fahnestock, D.J. Miller, Computational study of self- centering buckling-restrained braced frame seismic performance, Earthquake engineering & structural dynamics, 43 (2014) 1897-1914.

[4] J. Erochko, C. Christopoulos, R. Tremblay, H.J. Kim, Shake table testing and numerical simulation of a self-centering energy dissipative braced frame, Earthquake engineering & structural dynamics, 42 (2013) 1617-1635.

[5] D.J. Miller, L.A. Fahnestock, M.R. Eatherton, Development and experimental validation of a nickel–titanium shape memory alloy self-centering buckling-restrained brace, Engineering Structures, 40 (2012) 288-298.

[6] L.-H. Xu, X.-W. Fan, Z.-X. Li, Development and experimental verification of a pre-pressed spring self-centering energy dissipation brace, Engineering Structures, 127 (2016) 49-61.

[7] S. Zhu, Y. Zhang, Seismic analysis of concentrically braced frame systems with self-centering friction damping braces, Journal of Structural Engineering, 134 (2008) 121-131.

[8] A. Filiatrault, S. Cherry, Seismic design spectra for friction-damped structures, Journal of Structural Engineering, 116 (1990) 1334-1355.

[9] R.-H. Zhang, T. Soong, Seismic design of viscoelastic dampers for structural applications, Journal of Structural Engineering, 118 (1992) 1375-1392.

[10] N. Gluck, A. Reinhorn, J. Gluck, R. Levy, Design of supplemental dampers for control of structures, Journal of structural Engineering, 122 (1996) 1394-1399.

[11] I. Takewaki, Optimal damper placement for minimum transfer functions, Earthquake Engineering & Structural Dynamics, 26 (1997) 1113-1124.

[12] B. Wu, J.-P. Ou, T. Soong, Optimal placement of energy dissipation devices for three-dimensional structures, Engineering Structures, 19 (1997) 113-125.

[13] A. Shukla, T. Datta, Optimal use of viscoelastic dampers in building frames for seismic force, Journal of Structural Engineering, 125 (1999) 401-409.

[14] D.L. Garcia, A simple method for the design of optimal damper configurations in MDOF structures, Earthquake spectra, 17 (2001) 387-398.

[15] L. Moreschi, M. Singh, Design of yielding metallic and friction dampers for optimal seismic performance, Earthquake engineering & structural dynamics, 32 (2003) 1291-1311.

[16] D. Asahina, J.E. Bolander, S. Berton, Design optimization of passive devices in multidegree of freedom structures, 13th World Conf on Earthq Eng, 2004.

[17] O. Lavan, R. Levy, Optimal design of supplemental viscous dampers for linear framed structures, Earthquake engineering & structural dynamics, 35 (2006) 337-356.

[18] A.S. Kokil, M. Shrikhande, Optimal placement of supplemental dampers in seismic design of structures, Journal of Seismology and Earthquake Engineering, 9 (2007) 125-135.

[19] S. Sanghai, S. Khante, Seismic response of unsymmetric building with optimally placed friction dampers, Technology, 8 (2017) 72-88.

[20] E. Nobahar, B. Asgarian, O. Mercan, S. Soroushian, A post-tensioned self-centering yielding brace system: development and performance-based seismic analysis, Structure and Infrastructure Engineering, (Submitted for publication)

[21] A.T. Council, M.-A.E. Center, M.C.f.E.E. Research, P.E.E.R. Center, U.S.F.E.M. Agency, N.E.H.R. Program, Interim Testing Protocols for Determining the Seismic Performance Characteristics of Structural and Nonstructural Components, Federal Emergency Management Agency2007.

[22] M.F. Mazzoni S, Scott MH and Fenves GL (2009) Open system for earthquake engineering simulation user command-language manual-OpenSees version 2.0. Berkeley, CA: Pacific Earthquake Engineering Research Center, University of California.

[23] P.G. Somerville, Development of ground motion time histories for phase 2 of the FEMA/SAC steel project, SAC Joint Venture1997.

[24] B.G. Simpson, S.A. Mahin, Experimental and numerical investigation of strongback braced frame system to mitigate weak story behavior, Journal of Structural Engineering, 144 (2018) 04017211.

[25] FEMA 356. Prestandard and Commentary for the Seismic Rehabilitation of Buildings, Washington, D.C., 2000.

[26] ASCE/SEI (ASCE/Structural Engineering Institute). (2016).“Minimum design loads for buildings and other structures.”ASCE/SEI 7-16, VA.